Chinese Journal of Chemical Engineering 42 (2022) 415–423

Contents lists available at ScienceDirect

Chinese Journal of Chemical Engineering

journal homepage: www.elsevier.com/locate/CJChE

Full Length Article

Influence of coke rate on thermal treatment of waste selective catalytic reduction (SCR) catalyst during iron ore sintering

Pengnan Ma, Jiankang Wang, Hanxiao Meng, Laiquan Lv, Hao Fang, Kefa Cen, Hao Zhou *

State Key Laboratory of Clean Energy Utilization, Institute for Thermal Power Engineering, Zhejiang University, Hangzhou 310027, China

ARTICLE INFO

Article history:
Received 3 August 2020
Received in revised form 20 February 2021
Accepted 23 February 2021
Available online 8 May 2021

Keywords:
Flame front
Waste selective catalytic reduction (SCR) catalyst
Thermal treatment
Iron ore sintering

ABSTRACT

Waste selective catalytic reduction (SCR) catalyst as a hazardous waste has a significant impact on the environment and human health. In present study, a novel technology for thermal treatment of waste SCR catalyst was proposed by adding it to sinter mix for iron ore sintering. The influences of coke rate on the flame front propagation, sinter microstructure, and sinter quality during sintering co-processing the waste SCR catalyst process were studied. In situ tests results indicated the maximum sintering bed temperature increased at higher coke rate, indicating more liquid phase generated and higher airflow resistance. The sintering time was longer and the calculated flame front speed dropped at higher coke rate. Sinter microstructure results found the coalescence and reshaping of bubbles were more fully with increasing coke rate. The porosity dropped from 35.28% to 25.66%, the pore average diameter of large pores decreased from 383.76 μm to 311.43 μm. With increasing coke rate, the sinter indexes of tumbler index, productivity, and yield, increased from 33.2%, 9.2 $t \cdot m^{-2} \cdot d^{-1}$, 28.9% to 58.0%, 36.0 $t \cdot m^{-2} \cdot d^{-1}$, 68.9%, respectively. Finally, a comprehensive index was introduced to systematically assess the influence of coke rate on sinter quality, which rose from 100 to 200 when coke rate was increased from 3.5% (mass) to 5.5% (mass).

1. Introduction

In recent years, the rapid increase in NOx emissions has caused great concern. Selective catalytic reduction (SCR) technology is considered to be one of the most effective methods to reduce NOx emissions, which has been widely used in power plants and other stationary emitting sources for selective catalytic reduction of NOx by NH_3 [1]. The most commonly used SCR catalyst is TiO_2-WO_3/MoO_3-V_2O_5 system owing to the wide temperature window, high efficiency and durability. In the components of SCR catalyst, TiO_2 is the supporting oxide, V_2O_5 is the active component and WO_3/MoO_3 is the promoter [2,3]. The SCR catalyst can suffer deactivation in the bad operating environment and its lifespan is known to be about 3 years. The specific causes of deactivation can be divided into six categories: (1) poisoning, (2) fouling, (3) thermal degradation, (4) vapor compound formation and/or leaching accompanied by transport from the catalyst surface or particle, (5) vapor–solid and/or solid–solid reactions, and (6) attrition/crushing [4]. With the increasingly strict environmental protection requirements, a large amount of catalyst is used in SCR systems. After a long period of operation, a lot of coal-fired fly ash has been deposited on the surface of the waste SCR catalyst. The toxic substances contained in the waste SCR catalyst will contaminate the soil and groundwater, thereby affecting human health. At the same time, the V_2O_5 contained in the waste SCR catalyst is a toxic substance, and many countries define the waste SCR catalyst as hazardous waste. It is estimated that 150,000 m^3 of waste SCR catalyst will be produced annually in China [5]. Addressing the waste SCR catalyst has been an increasingly hot issue.

The main waste SCR catalyst treatment methods can be divided into the following types: (1) landfill [3,6,7]; (2) regeneration [8–10]; (3) recovery valuable metals [6,11–13]; (4) high temperature melting and solidification heavy metals [14]; (5) co-combustion with coal [15]. Landfill is the most common method among the treatment methods mentioned above. However, landfill will cause great damage to the environment. Although the lifespan of the waste SCR catalyst can be extended by regeneration, it will always be abandoned in the end and needs to be treated. In the process of recovering precious metals, the researchers only focus on the extraction rate of valuable metals such as V, W, Ti. The remaining part of the waste SCR catalyst which can cause secondary pollution to the environment is often neglected. High temperature melting and solidification heavy metals is a feasible method, but the energy

* Corresponding author.
E-mail address: zhouhao@zju.edu.cn (H. Zhou).

https://doi.org/10.1016/j.cjche.2021.02.029

consumption is too high. A more appropriate approach is to use the existing high-temperature processes in the industry. The most common high-temperature processes in the industry are mainly pulverized coal combustion process of coal-fired power plant and iron ore sintering process in ironmaking. Wang [15] reported a method of co-combustion of waste SCR catalyst with coal. However, iron ore sintering process has not been reported to treat waste SCR catalyst. Up to 2017, there are about 900 sintering machines with an area of 116 thousand m^2 and annual sinter production is 850 million tons in China [16]. It is a potential way to treat waste SCR catalyst.

In iron ore sintering process, the fine-grained iron ore needs to be granulated into large particles and agglomerated to form iron ore sinter which are then sent to the blast furnace. As the main component of waste catalyst, TiO_2 can protect the hearth of blast furnace [17]. And the waste SCR catalyst contains SiO_2, Al_2O_3, Fe_2O_3, CaO, MgO, which is similar to the sintering raw materials. Moreover, most of the organic compounds generated by adding waste SCR catalyst can be decomposed during the sintering. Therefore, it is reasonable to dispose of waste SCR catalyst during iron ore sintering.

In iron ore sintering process, 4% (mass) coke supplies about 80% heat for melting raw materials and converting the green bed to sintered bed [18]. The coke combustion changes the structure of the sintering bed and affects the formation of mineral phase components, which has a great influence on sinter quality. Therefore, it is not surprised that a minor change in coke level would have a significant influence on combustion behavior, flame front propagation, and sintering performance.

In present study, the influence of coke rate on thermal treatment of waste SCR catalyst in iron ore sintering is investigated. The effects of coke rate on the flame front propagation, sinter microstructure, sinter indexes are studied. Then, a comprehensive index is introduced to assess the influence of coke rate on thermal treatment of waste SCR catalyst in iron ore sintering.

2. Material and Methods

2.1. Material

In this investigation, all the raw materials were divided by a rotary divider to ensure the uniformity. Table 1 gives the chemical compositions of sintering raw materials, including five iron ores, limestone and dolomite, and coke.

The waste SCR catalyst comes from a power plant in eastern China. The chemical component of waste SCR catalyst is shown in Table 2. In the waste SCR catalyst, TiO_2 is the main component, accounting for 70% of the total mass of the waste SCR catalyst. TiO_2 can protect the hearth layer of the blast furnace. In addition, there are a considerable amount of SiO_2 and Al_2O_3 in waste SCR catalyst owing to a large amount of fly ash absorbed during operation.

Five schemes are designed to investigate the influence of coke rate on thermal treatment of waste SCR catalyst in iron ore sintering. Table 3 gives the detailed ore blend proportion, sinter condition, and experimental schemes. The basicity and the mass fraction of MgO are adjusted to 1.9 and 1.7% (mass) to meet the fluidity requirements of blast furnace slag. The granulation moisture is set to ~6.0% (mass) and return fines is 25% (mass). According to our previous research [20], when the level of waste SCR catalyst added was 2% (mass), the sinter indexes including TI, productivity, yield, and FFS all decreased slightly, but it is comparable to that of 0% waste SCR catalyst added. When the level of waste SCR catalyst was further increased, the sintering index decreased significantly. Therefore, adding 2% (mass) waste SCR catalyst is feasible during iron ore sintering process. The mass fraction of coke changes from 3.5% (mass) to 5.5% (mass).

Table 3
Ore blend proportion, sinter conditions and experimental schemes

	Ore blend proportion/% (mass)
AUS1 ores	16.67
AUS2 ores	16.67
AUS3 ores	33.33
BRA1 ores	16.67
BRA2 ores	16.67
	Sinter conditions/% (mass)
Moisture	6.0
Return fines	25
Basicity (CaO/SiO_2)	1.9
MgO	1.7
Waste catalyst	2
Scheme	**Coke rate/% (mass)**
1	3.5
2	4.0
3	4.5
4	5.0
5	5.5

Table 1
Chemical compositions of sintering raw materials (% (mass)) [19]

Item	TFe	Al_2O_3	SiO_2	MgO	CaO	P	S	LOI1000[①]
AUS1 ores	60.62	2.25	4.45	0.08	0.05	0.07	0.03	5.91
AUS2 ores	62.39	2.23	4.28	0.13	0.15	0.08	0.02	3.51
AUS3 ores	58.07	1.26	5.09	0.07	0.08	0.04	0.02	10.20
BRA1 ores	64.98	1.26	2.36	0.07	0.06	0.02	0.01	2.03
BRA2 ores	64.31	0.79	5.42	0.17	0.09	0.03	0.01	1.09
Limestone	2.91	0.79	2.16	0.36	51.32	0.01	0.07	40.80
Dolomite	0.35	0.58	2.26	19.45	31.45	0.01	0.03	45.50
Coke	1.07	4.32	6.11	0.04	0.62	0.03	0.01	86.85

① LOI1000: Loss on ignition at 1000 °C in air.

Table 2
Chemical composition of waste SCR catalyst/% (mass) [20]

TiO_2	SiO_2	Al_2O_3	V_2O_5	MoO_3	Fe_2O_3	CaO	MgO	K_2O	Na_2O	LOI1000[①]
70.06	7.17	5.79	3.75	1.58	0.76	0.34	0.80	0.53	0.79	11.48

① LOI1000: Loss on ignition at 1000 °C in air.

2.2. Methods

2.2.1. Sinter pot test

As shown in Fig. 1, a laboratory scale sinter pot was conducted to simulate the industrial sintering process. The diameter and height of the sinter pot are 120 mm and 650 mm, respectively. The weighted and mixed raw materials were subjected to a two-stage granulating drum first, that is, dry mixing for 1 min followed by wet mixing for 10 min. Then, ~17 kg granules were charged into the sinter pot to create a packed bed on a 1 kg hearth layer of 6.3–8 mm sinter particles placed on the bottom of sinter pot in advance. The top layer of the packed bed was ignited for 90 s by a natural gas burner at the temperature of ~1200 °C and negative pressure of 6 kPa. After the flame front was established, the natural gas igniter was removed and a hood was placed on the sinter pot. The negative pressure was raised to 16 kPa during sintering. The flame front propagated down the bed under the suction of the draught fan. The inlet airflow rate was measured by a hot wire anemometer installed in the middle of the hood, the accuracy of which is 0.01 $m \cdot s^{-1}$. Five pressure transmitters were installed at 100 mm, 200 mm, 400 mm, 500 mm, 600 mm heights from the top of the sinter pot to record the pressure fields of the sintering bed. An S-type thermocouple located at 300 mm height was used to measure the sintering bed temperature. The windbox temperature was monitored by an R-type thermocouple. The sintering process was considered to be finished when the windbox temperature reached its maximum value.

The typical sintering indexes, including tumbler index (TI), flame front speed (FFS), yield, and productivity were tested. Yield is the mass fraction of the sinter particles larger than 5 mm after sieving, with the mass of hearth layer subtracted, %. Productivity is the amount of sinter product per unit area and per unit time, $t \cdot m^{-2} \cdot d^{-1}$. Tumbler index is a measurement of sinter strength, which indicates the mass fraction of sinter particles above 6.3 mm after drum test, %.

2.2.2. Microstructure characterization

In iron ore sintering process, the structural transformation of the sinter bed is caused by the coalescence of gas channels at the flame front, which also determines the microstructure of the sinter. In the present study, the representative sinters were broken into 6.3–8 mm and inlaid in epoxy resin for more than 12 hours. The solidify samples are shown in Fig. 2(a). The surface containing pore structure information of the sinter was cut and polished by a Struers cutting machine and then polished using a Struers Tegrapo-35. After that, the sinter was placed under a Zeiss Axioskop reflective metallographic microscope shown in Fig. 2(b) to analyze the pore structure information of the sinter. An Axiocam MRc 5 CCD camera was used to take photos of the samples. The 2.5 × objective lens and 10 × eyepiece are used to observe the pore structure of the samples. The captured about 30 images were analyzed by Axiovisio software according to different gray values setting.

Fig. 3(a) and (b) shows the microstructure of the sinter and image background denoising. And three important parameters of the pore structure were measured and analyzed, namely area, diameter and circle factor of pores.

3. Results and Discussion

3.1. Influence of coke rate on flame front propagation

Fig. 4(a) and (b) shows the *in situ* sintering bed temperature at 300 mm height and negative pressures at different bed heights, inlet airflow rate, windbox temperature and pressure at 3.5% (mass) and 5.5% (mass) coke rate conditions of sinter pot tests. The successive rapid drop in the negative pressure of sintering bed indicates the propagation of the flame front in a self-sustaining manner. The sintering bed temperature is maintained at 60 °C before the flame front arrives, which corresponds to the water evaporation temperature near the flame front. The evaporated water condenses in the lower bed owing to the lower temperature than dew point. When the flame front is approaching, the material layer is heated from water evaporation temperature to maximum temperature at 500–700 $°C \cdot min^{-1}$. However, a rapid drop of sintering bed temperature could be observed after the maximum sintering bed temperature, indicating that the flame front is very thin. Both the maximum sintering bed temperature and windbox temperature increase at higher coke rate. The sintering time, namely the interval from the start of ignition until the windbox temperature reaches the maximum, is longer and the cal-

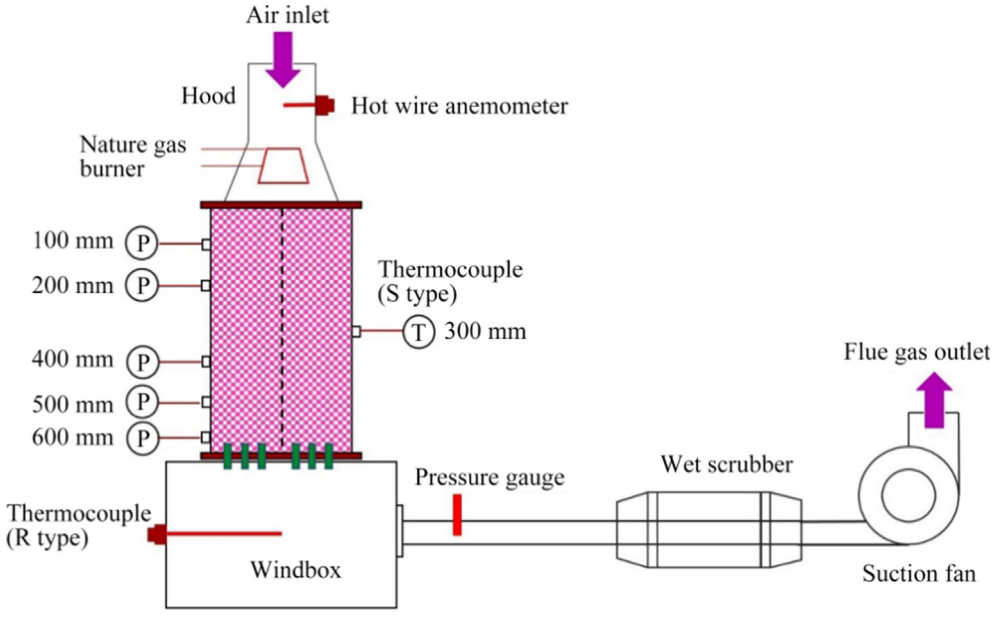

Fig. 1. Schematic diagram of the sinter pot system.

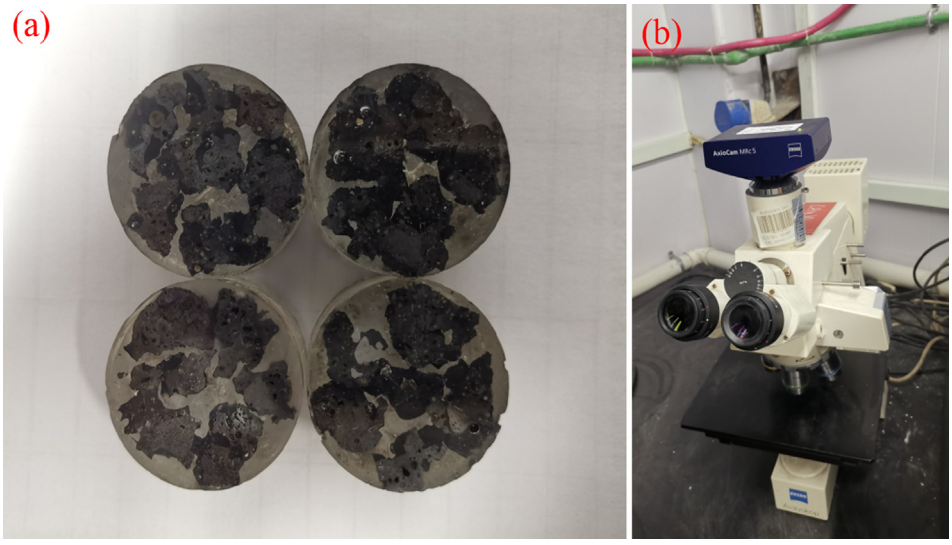

Fig. 2. (a) Sintered samples mounted in epoxy resin. (b) Metallographic microscope equipped with a CCD camera.

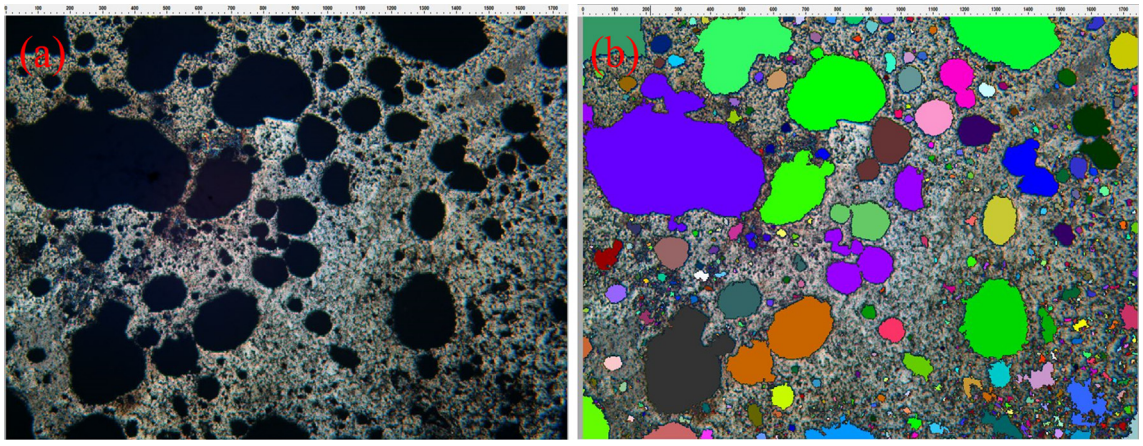

Fig. 3. (a) Sinter microstructure. (b) Pore extraction and denoising.

culated flame front speed drops at higher coke rate. The sintering bed can be simplified into sintered zone, high temperature zone and over-wetted zone [21]. The resistance of high temperature zone is the largest, followed by over-wetted zone and the sintered zone is the smallest. As the flame front propagates downward, there is a one-to-one replacement between the over-wetted zone and the sintered zone. The thickness of sintered zone gradually increases while the thickness of over-wetted zone gradually decreases. The thickness of high temperature zone increases gradually due to the heat accumulation effect of the bed, and the increase of resistance in high temperature zone almost counteracts the decrease of resistance caused by the one-to-one replacement between the over-wetted zone and the sintered zone. Therefore, the airflow rate through the sintering bed remains relatively constant [22]. The inlet airflow rate increases rapidly once the flame front burns through the sintering bed, which indicates that the flame front has a dominant influence on the inlet airflow rate.

The sintering bed negative pressures drop slowly before the flame front arrives. And the decline rate is faster at higher coke rate. The bed negative pressures drop rapidly when the flame front travels away. For the 100 mm height of sintering bed at 5.5% (mass) coke rate, the negative pressure is zero, *i.e.* ambient pressure due to the greater shrinkage at higher coke rate. When the flame front breaks through the sintering bed, the negative pressures increase rapidly. The flame front has a controlling effect on the resistance of the whole sintering bed during iron ore sintering process [23]. When the flame front burns through the bed, the thickness of the flame front decreases gradually, resulting in the decrease of the resistance in the bed. For a certain position in the bed, the pressure loss drops due to the decrease of bed resistance, so the negative pressure value increases.

Fig. 5 shows the derivatives of negative pressure value versus time at different bed height locations assuming the flame front speed is constant, which denote the transient pressure drop along the sintering bed. As the flame front travels down the bed, the accumulated heat and maximum sintering bed temperature become greater, indicating more liquid phase generated and higher airflow resistance [24]. The corresponding absolute value of the pressure drop is larger at lower sintering bed.

3.2. Influence of coke rate on sinter microstructure properties

In general, a granulated green bed characterizes a porosity of 30%–40% [25]. When the flame front arrives, a certain proportion of voids will be trapped in molten liquid phase as bubbles. Since the melt-gas system is always moving towards a minimum energy

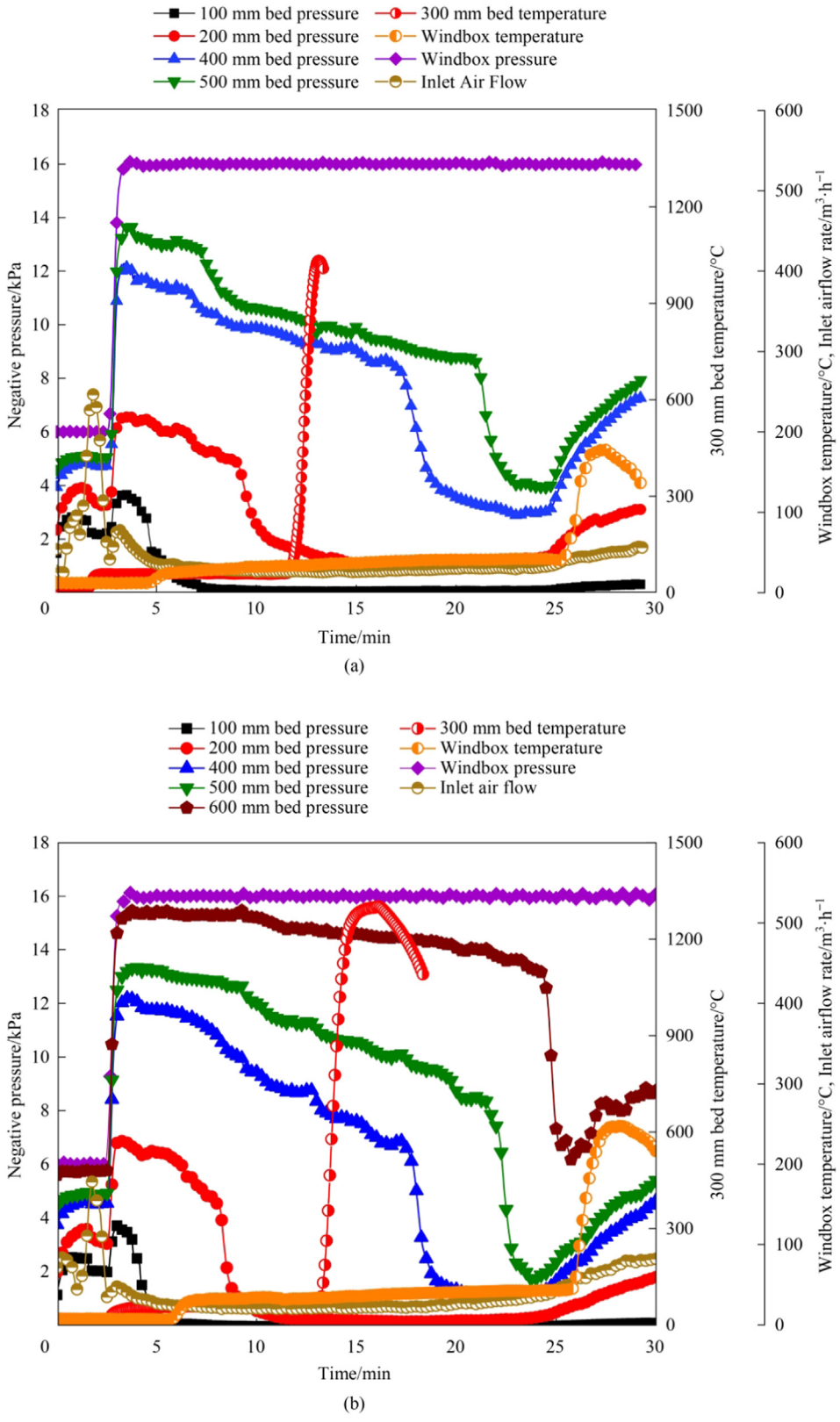

Fig. 4. In situ sintering bed negative pressures and temperature, windbox negative pressure and temperature, and inlet airflow rate at (a) 3.5% (mass) coke rate and (b) 5.5% (mass) coke rate.

state, the bubbles will reshape and coalesce to reduce the surface area meanwhile lower the energy of the system [26]. The coalescence and reshaping of bubbles and melts in flame front result in the structure transformation of the sintering bed. As the flame front travels away, the bubbles gradually cool down and become pores. The tumbler index and yield of the sinters are largely affected by the inherent strength and structure of the bonding phase. However, it is hard to continuously track the structural

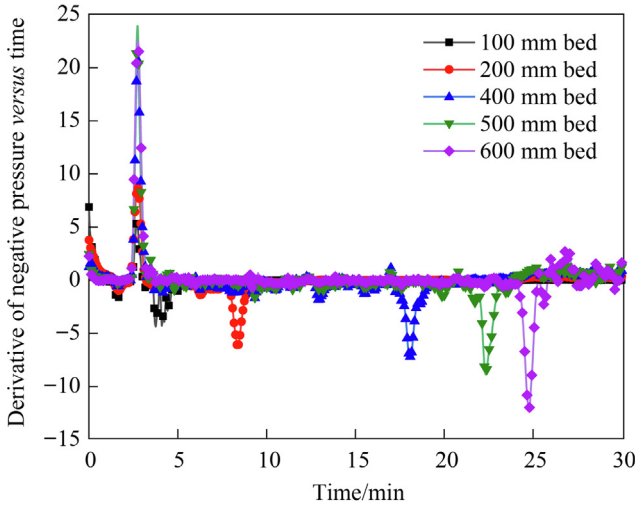

Fig. 5. Derivatives of negative pressure value *versus* time at different bed height locations (Scheme 5: 5.5% (mass) coke rate).

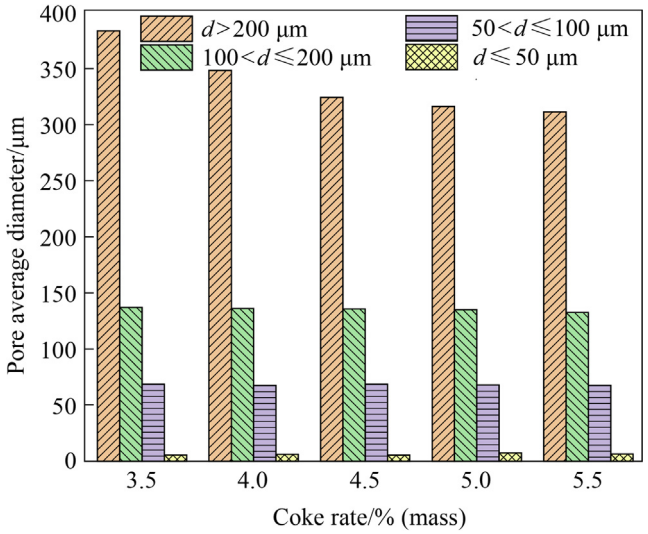

Fig. 7. Effect of coke rate on pore average diameter of sinter.

changes of sintering bed in iron ore sintering process. Studying the product sinter particles is an easier method to assess the coalescence and reshaping degree of the melt and bubbles. Since coalescence and reshaping result in changes of the properties of bubbles in molten liquid phase, pore parameters could reflect the coalescence degree of sinter materials in the flame front.

Fig. 6 illustrates the porosity of the sinter varying coke rate. The porosity decreases from 35.28% to 25.66% when coke rate increases from 3.5% (mass) to 5.5% (mass). Generally, higher coke rate means more heat is input into the sintering bed. The sintering bed maximum temperature and residence time above 1100 °C increase as higher coke rate is applied, resulting in more melts formation, lower apparent viscosity, and higher fluidity of molten liquid phase [27]. The coalescence of bubbles is easier to achieve, therefore, more completely. When the bubbles coalesce to a certain size, they will be expelled from the melts, resulting in the formation of a denser sinter. In addition, flame front speed decreases and sintering time lengthens with more coke added, there are more time for bubbles to undergo coalescence and densification.

The pore properties were found to depend on pore size (d) and the measurement results are divided into 4 categories: fine ($d \leq 50$ μm), small (50 μm$<d\leq$100 μm), medium (100 μm$<d\leq$200 μm), large ($d>200$ μm). Fig. 7 shows the pore average diameter of the sinter particles, which reflects the melts properties supporting bubbles coalescence. It can be observed that the average diameter of large pores has a descending trend with increasing coke rate. The pore average diameter decreases from 383.76 μm for 3.5% (mass) coke level to 311.43 μm for 5.5% (mass) coke level. With higher sintering bed temperature, the coalescence of bubbles will be more fully. The bubbles would be expelled from the melts owing to buoyancy forces. The larger bubbles leave the liquid phase more easily because of greater buoyancy forces. Besides, the decrease of apparent viscosity also provides an advantage for bubbles to coalesce and leave the liquid phase.

The bubbles in the melts will reshape to more spherical shape so that reduce the system energy level. In present investigation, the circle factor represents how close the bubble is to a spherical shape. And it can indicate the influences of two opposing forces, one is the surface tension that makes the bubble more spherical, and the other is the viscous force that prevents this transition. Fig. 8 indicates that the circle factor of smaller pores is greater. The driving force of bubbles reshaping is a function of $2\gamma/r$, where γ is surface tension and r is radius of bubbles. It is obvious that small bubbles will reshape more easily than large bubbles. The cir-

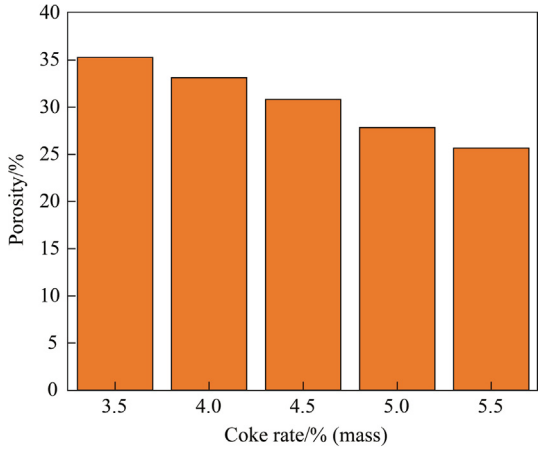

Fig. 6. Effect of coke rate on porosity of sinter.

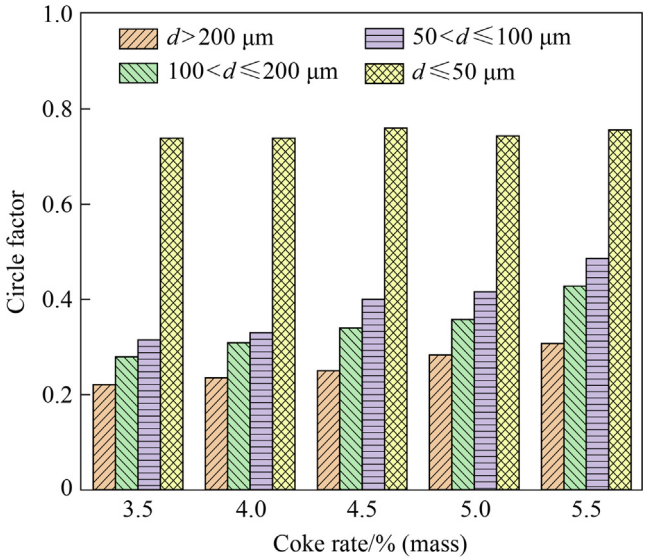

Fig. 8. Effect of coke rate on pore circle factor of sinter.

cle factor of the pores with a diameter greater than 50 μm increases with increasing coke rate. The longer sintering time provides more opportunities for bubble to reshape.

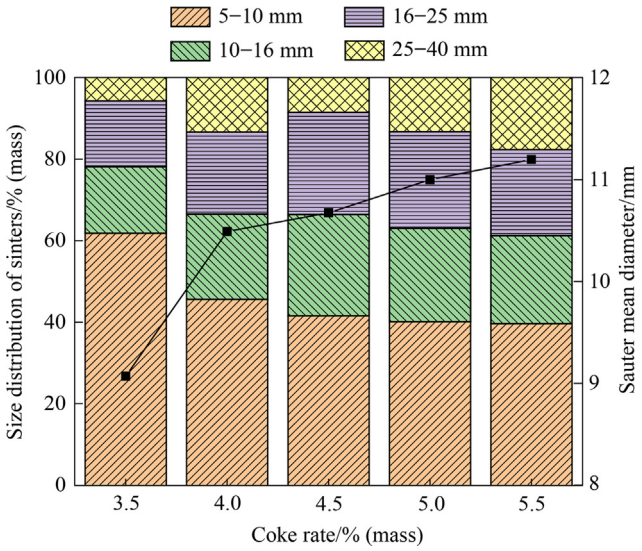

Fig. 9. Effect of coke rate on size distribution of sinters.

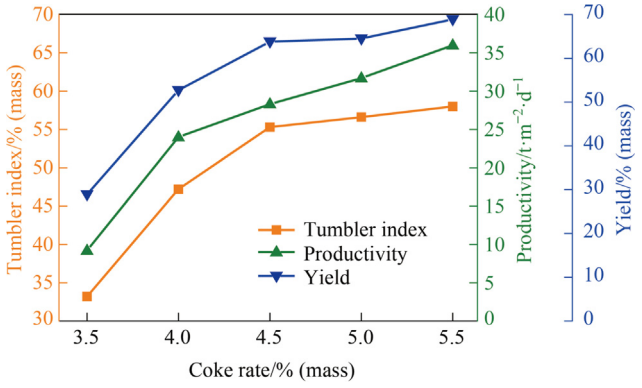

Fig. 10. Effect of coke rate on sinter indexes.

3.3. Influence of coke rate on sinter quality and further application

The sinter quality is affected by coke rate. Fig. 9 gives the size distribution of sinter particles. It can be found that +10 mm sinter particles show an increasing trend with increasing coke rate. The sauter mean diameter of sinter particles increases from 9.1 mm for 3.5% (mass) coke level to 11.2 mm for 5.5% (mass) coke level. Generally, more bonding phase will be formed in high temperature zone with increasing coke rate, which is conducive to the improvement of sintering strength [22]. Therefore, the proportion of sinter with lager particle size is higher. Fig. 10 shows the sinter indexes at different coke rate. All the sinter indexes increase as more coke is applied in iron ore sintering process. Sinter indexes of tumbler index, productivity, yield increase from 33.2%, 9.2 $t \cdot m^{-2} \cdot d^{-1}$, 28.9% to 58.0%, 36.0 $t \cdot m^{-2} \cdot d^{-1}$, 68.9% when the coke level increases from 3.5% (mass) to 5.5% (mass). As can be seen in Fig. 4, the maximum sintering bed temperature increases with greater coke rate, resulting in more liquid phase formation. In addition, Fig. 6 also indicates that a denser sinter is obtained as more coke is applied. The more melts and denser sinter product are both conducive to improving the sinter strength.

Fig. 11 gives the sinter microstructure at different coke rate. Compared with the condition of 3.5% (mass) coke rate, more acicular calcium ferrite is formed while less primary hematite exists at 5.5% (mass) coke rate. In addition, excessive porosity at low coke rate can deteriorate sinter strength. The more calcium ferrite and denser sinter product are both conducive to improving the sinter strength.

In this work, a comprehensive index [28] is introduced to systematically evaluate the influence of coke rate on sinter quality. The first group of comprehensive index is quantized to 100 to make comparative analysis more easily. The comprehensive index is conducted by:

$$R_i = r_i - r_1 + 100 \tag{1}$$

$$R_1 = 100 \tag{2}$$

where R_i is the comprehensive index, r_i is the composite index and can be expressed as:

$$r_i = \sum_{j=1}^{m} \alpha_j x_{ij} (i = 1, 2, \cdots, n;\ j = 1, 2, \cdots, m) \tag{3}$$

$$r_i \geqslant 0\ (i = 1, 2, \cdots, n) \tag{4}$$

where α_j is the unit range coefficient and could be calculated by:

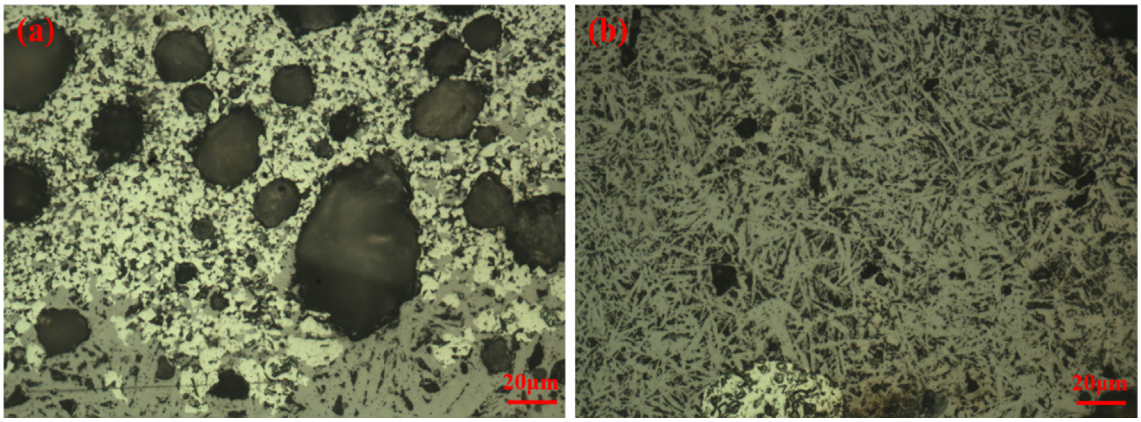

Fig. 11. Effect of coke rate on sinter microstructure. (a) 3.5% (mass) coke rate, (b) 5.5% (mass) coke rate.

$$\alpha_j = \frac{S_j}{D_j} \tag{5}$$

where S_j is the weight coefficient of sinter indexes

$$\sum_j S_j = 100\ (j = 1, 2, \cdots, m) \tag{6}$$

$S_1 = 40$, $S_2 = 30$, $S_3 = 30$ are given by Panzhihua Iron and Steel Company of China based on years of experience.D_j is the range

$$D_j = (x_{ij})_{\max} - (x_{ij})_{\min} \tag{7}$$

where x_{i1}, x_{i2}, x_{i3} are productivity, yield, and tumbler index, respectively.

The calculation results are given in Fig. 12. The comprehensive index rises from 100 to 200 when coke rate increases from 3.5% (mass) to 5.5% (mass). More coke applied into iron ore sintering process is conducive to sinter quality. However, the balance between sinter quality and fuel consumption should be considered in practical industrial applications.

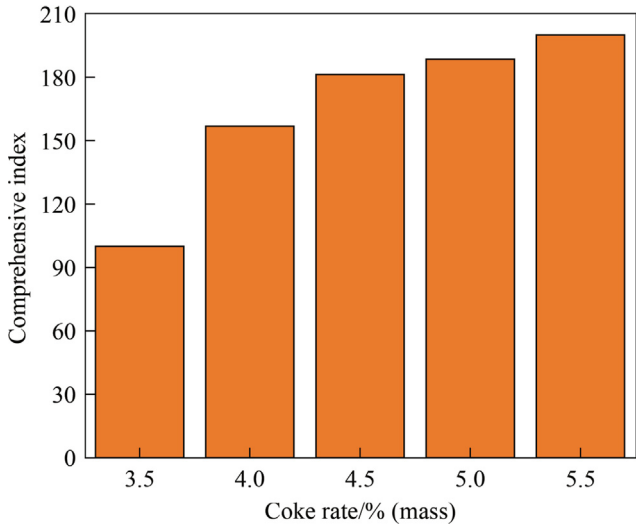

Fig. 12. Effect of coke rate on comprehensive index.

Fig. 13 illustrates the schematic diagram of practical application of sintering co-processing the waste SCR catalyst. The waste SCR catalyst is directly added to sinter raw materials without any pre-processing steps. This technology is easy to realize without any additional equipment. The sintering co-processing the waste SCR catalyst could promote the coordinated development of steel plant and local city.

4. Conclusions

This study aims at revealing the influence of coke rate on thermal treatment of waste SCR catalyst in iron ore sintering. The influences of coke rate on the flame front propagation, sinter microstructure, sinter indexes are studied. The following conclusions can be obtained from this study:

(1) Both the maximum sintering bed temperature and windbox temperature increase at higher coke rate, indicating more liquid phase generated and higher airflow resistance. The absolute value of the pressure drop is larger at lower sintering bed. The sintering time is longer and the flame front speed drops at higher coke rate.

(2) With increasing coke rate, the coalescence and reshaping of bubbles will be more fully. The porosity decreases from 35.28% to 25.66% when coke rate increases from 3.5% (mass) to 5.5% (mass). And the pore average diameter decreases from 383.76 μm for 3.5% (mass) coke level to 311.43 μm for 5.5% (mass) coke level. The circle factor of the pores with the diameter greater than 50 μm increases with increasing coke rate. All these result in a denser sinter.

(3) The sauter mean diameter of sinter particles increases from 9.1 mm for 3.5% (mass) coke level to 11.2 mm for 5.5% (mass) coke level. Sinter indexes of tumbler index, productivity, yield increase from 33.2%, 9.2 $t \cdot m^{-2} \cdot d^{-1}$, 28.9% to 58.0%, 36.0 $t \cdot m^{-2} \cdot d^{-1}$, 68.9% when the coke level increases from 3.5% (mass) to 5.5% (mass). The comprehensive index rises from 100 to 200 when coke rate increases from 3.5% (mass) to 5.5% (mass).

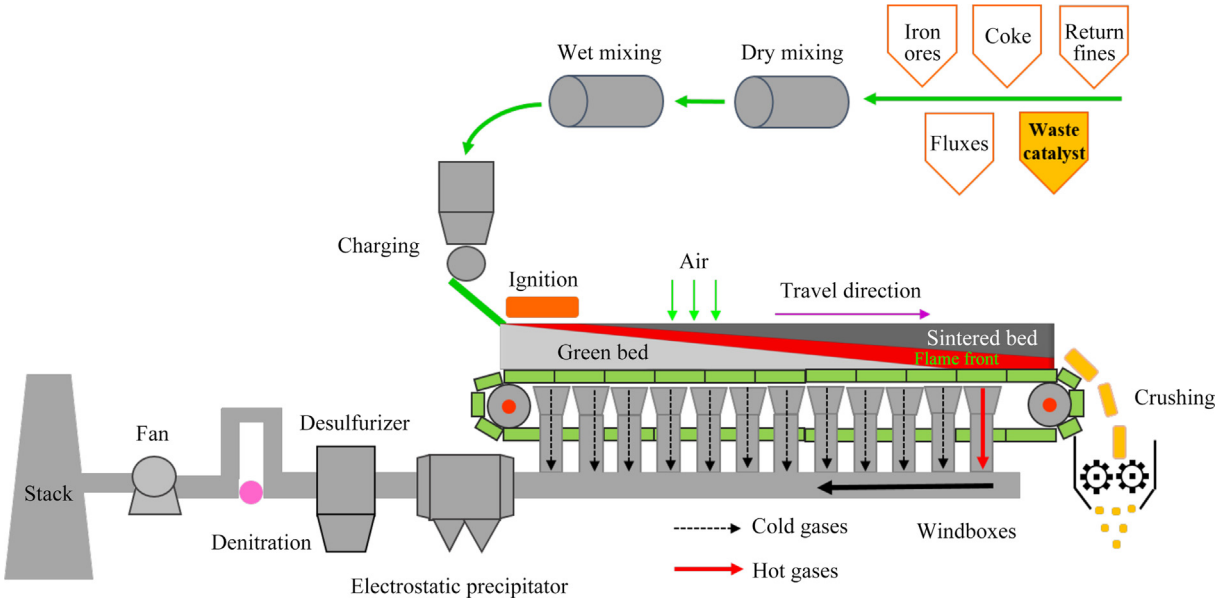

Fig. 13. Practical application of sintering co-processing the waste SCR catalyst.

Declaration of Competing Interest

The authors declare that they have no known competing financial interests or personal relationships that could have appeared to influence the work reported in this paper.

Acknowledgements

This work was supported by the National Natural Science Foundation of China (52036008).

References

[1] Y.-J. Shi, H. Shu, Y.-H. Zhang, H.-M. Fan, Y.-P. Zhang, L.-J. Yang, Formation and decomposition of NH_4HSO_4 during selective catalytic reduction of NO with NH_3 over V_2O_5-WO_3/TiO_2 catalysts, *Fuel Process. Technol.* 150 (2016) 141–147.
[2] I.H. Choi, G. Moon, J.Y. Lee, R.K. Jyothi, Alkali fusion using sodium carbonate for extraction of vanadium and tungsten for the preparation of synthetic sodium titanate from spent SCR catalyst, *Sci. Rep.* 9 (1) (2019) 12316.
[3] I.-H. Choi, H.-R. Kim, G. Moon, R.K. Jyothi, J.-Y. Lee, Spent V_2O_5-WO_3/TiO_2 catalyst processing for valuable metals by soda roasting-water leaching, *Hydrometallurgy* 175 (2018) 292–299.
[4] M. Argyle, C. Bartholomew, Heterogeneous catalyst deactivation and regeneration: a review, *Catalysts* 5 (1) (2015) 145–269.
[5] X. Zhao, X. Cheng, J. Hou, Development report on desulfurization and denitration industry in 2017, *China Eevironmental Prot. Ind.* 7 (2018) 10–24.
[6] I.H. Choi, G. Moon, J.Y. Lee, R.K. Jyothi, Hydrometallurgical processing of spent selective catalytic reduction (SCR) catalyst for recovery of tungsten, *Hydrometallurgy* 178 (2018) 137–145.
[7] I.H. Choi, G. Moon, J.Y. Lee, R.K. Jyothi, Extraction of tungsten and vanadium from spent selective catalytic reduction catalyst for stationary application by pressure leaching process, *J. Clean. Prod.* 197 (2018) 163–169.
[8] X. Shang, G. Hu, C. He, J. Zhao, F. Zhang, Y. Xu, Regeneration of full-scale commercial honeycomb monolith catalyst, *J. Ind. Eng. Chem.* 18 (2012) 513–519.
[9] Y.D. Xue, Y. Zhang, Y. Zhang, S.L. Zheng, Y. Zhang, W. Jin, Electrochemical detoxification and recovery of spent SCR catalyst by in situ generated reactive oxygen species in alkaline media, *Chem. Eng. J.* 325 (2017) 544–553.
[10] M. Li, B. Liu, X.R. Wang, X.B. Yu, S.L. Zheng, H. Du, D. Dreisinger, Y. Zhang, A promising approach to recover a spent SCR catalyst: deactivation by arsenic and alkaline metals and catalyst regeneration, *Chem. Eng. J.* 342 (2018) 1–8.
[11] H.I. Kim, G. Moon, I. Choi, J.Y. Lee, R.K. Jyothi, Hydrometallurgical process development for the extraction, separation and recovery of vanadium from spent desulfurization catalyst bio-leach liquors, *J. Clean. Prod.* 187 (2018) 449–458.
[12] Q.J. Zhang, Y.F. Wu, T.Y. Zuo, Titanium extraction from spent selective catalytic reduction catalysts in a NaOH molten-salt system: Thermodynamic, experimental, and kinetic studies, *Metall. Mater. Trans. B* 50 (1) (2019) 471–479.
[13] B.T. Ma, Z.F. Qiu, J. Yang, C.H. Qin, J.L. Fan, A.S. Wei, Y.J. Li, Recovery of nano-TiO_2 from spent SCR catalyst by sulfuric acid dissolution and direct precipitation, *Waste Biomass Valoriz.* 10 (10) (2019) 3037–3044.
[14] H. Zhou, X.T. Guo, M.X. Zhou, Influence of different additives on harmless melting treatment of waste SCR catalysts, *J. Chin. Soc. Power Eng.* 37 (12) (2017) 999–1006.
[15] L.L. Wang, S. Su, M.X. Qing, Z.J. Dai, Z.J. Sun, L.J. Liu, Y. Wang, S. Hu, K. Xu, J. Xiang, Melting solidification and leaching behaviors of V/As during co-combustion of the spent SCR catalyst with coal, *Fuel* 252 (2019) 164–171.
[16] Ministry of Ecology and Environment of the People's Republic of China, Letter on Soliciting Opinions on 20 National Pollutant Discharge Standards (Draft for Comment) which including Emission Standard of Air Pollutants for Sintering and Pelletizing of Iron and Steel Industry (2017) [2020-7-22]. http://www.mee.gov.cn/gkml/hbb/bgth/201706/W020170615549538261241.pdf.
[17] J. Mochón, M.J. Quintana, I. Ruiz-Bustinza, R.G. Ojeda, E.M. Garcia, M.A.B. Fernández, L.F.V. González, Protection mechanisms for blast furnace crucible using titanium oxides, *Metall. Mater. Eng.* 18 (3) (2012) 195–201.
[18] J.P. Zhao, C.E. Loo, R.D. Dukino, Modelling fuel combustion in iron ore sintering, *Combust. Flame* 162 (4) (2015) 1019–1034.
[19] H. Zhou, Z.H. Liu, M. Cheng, M.X. Zhou, R.P. Liu, Influence of coke combustion on NOx emission during iron ore sintering, *Energy Fuel* 29 (2) (2015) 974–984.
[20] H. Zhou, P.N. Ma, Z.Y. Lai, Y.H. Zuo, Y.J. Xing, H. Shi, K.F. Cen, Harmless treatment of waste selective catalytic reduction catalysts during iron ore sintering process, *J. Clean. Prod.* 275 (2020) 122954.
[21] C.E. Loo, J.C.M. Leaney, Characterizing the contribution of the high-temperature zone to iron ore sinter bed permeability, *T. I. Min. Metall. C* 111 (2002) 11–17.
[22] H. Zhou, M. Zhou, P. Ma, M. Cheng, Experimental investigation on the flame front resistance of gas channel growth with melt formation in iron ore sinter beds, *Proc. Combust. Inst.* 37 (2019) 4607–4615.
[23] H. Zhou, M. Zhou, Z. Liu, M. Cheng, K. Qiu, K. Cen, Factors controlling high-Temperature zone resistance to airflow during iron ore sintering, *ISIJ Int.* 55 (2015) 2556–2565.
[24] H. Zhou, M.X. Zhou, M. Cheng, W.S. Guo, K.F. Cen, Experimental study and X-ray microtomography based CFD simulation for the characterization of pressure drop in sinter bed, *Appl. Therm. Eng.* 112 (2017) 811–819.
[25] H. Zhou, Z.H. Liu, M. Cheng, R.P. Liu, K.F. Cen, Effect of flame-front speed on the pisolite-ore sintering process, *Appl. Therm. Eng.* 75 (2015) 307–314.
[26] C.E. Loo, W. Leung, Factors influencing the bonding phase structure of iron ore sinters, *ISIJ Int.* 43 (9) (2003) 1393–1402.
[27] D.M. Liu, G. Evans, C.E. Loo, Iron ore sinter structure development under realistic thermal conditions, *Chem. Eng. Res. Des.* 130 (2018) 129–137.
[28] M. Zhou, S.-T. Yang, T. Jiang, X.-X. Xue, Influence of MgO in form of magnesite on properties and mineralogy of high chromium, vanadium, titanium magnetite sinters, *Ironmak. Steelmak.* 42 (3) (2015) 217–225.